Available online at www.sciencedirect.com

ScienceDirect

Procedia CIRP 57 (2016) 545 – 550

www.elsevier.com/locate/procedia

49th CIRP Conference on Manufacturing Systems (CIRP-CMS 2016)

Detection of workpiece shape deviations for tool path adaptation in robotic deburring systems

Alexander Kuss[a,*], Manuel Drust[a], Alexander Verl[b]

[a] *Fraunhofer Institute for Manufacturing Engineering and Automation IPA, Nobelstrasse 12, 70569 Stuttgart, Germany*

[b] *Institute for Control Engineering of Machine Tools and Manufacturing Units ISW, University of Stuttgart, Seidenstrasse 36, 70174 Stuttgart, Germany*

[*] Corresponding author. Tel.: +49-711-970-1297; fax: +49-711-970-1008. *E-mail address:* alexander.kuss@ipa.fraunhofer.de

Abstract

Robotic systems have the potential to automate deburring processes along edges of arbitrarily shaped workpieces. The desired robot movement can be realized by proper trajectory planning using the computer-aided design (CAD) model of the manufactured workpiece. A fundamental problem is that geometric shape deviations between the nominal CAD model and the manufactured parts might be beyond acceptable limits for correct execution of the deburring process. This paper proposes a novel, easy to implement and practical approach to detect shape deviations of workpieces for automatic adaptation of robotic deburring processes. The approach only uses dimensional tolerance specifications of the manufactured part provided by the product design to derive possible variations of the workpiece geometry model. A matching process is performed between point clouds for each of the considered variants and a measured point cloud from the manufactured workpiece using an Iterative Closest Point (ICP) approach. Resulting point distances are used for evaluation of shape similarity between the compared point clouds. Finally, the most similar geometry model is identified for subsequent trajectory planning and workpiece localization. Experimental validation is performed by an industrial robot equipped with a stereo camera for shape sensing and a milling tool for subsequent execution of a deburring process. The results demonstrate the effectiveness and practicality of the proposed approach in industrial applications and an increased deburring quality.

Peer-review under responsibility of the scientific committee of the 49th CIRP Conference on Manufacturing Systems

Keywords: Deburring; Industrial Robot System; Shape Deviation; CAD Model

1. Introduction

Robotic deburring systems based on machining processes have been investigated for several years to overcome quality and ergonomic problems of a manual process execution. Especially for large and complex workpieces, robots represent a flexible and cost-effective solution for an automated deburring process [1]. However, positioning or shape errors of the deburring workpiece can cause an incorrect process execution resulting in insufficient deburring quality and high forces on the robot end effector.

To overcome these drawbacks, extensive research has been done on active control of the contact forces between deburring tool and workpiece to adapt the tool path [2], [3], [4]. Here, the deburring quality however depends on the dynamic behaviour of the complete robot cell and on shape deviations along the deburring contour, like e.g. varying burr size. Other approaches try to generate the tool path without prior knowledge about the workpiece geometry model by using teaching methods [5], [6], [7], computer vision [8], [9], [10] or combined methods [11]. The deburring contour is reconstructed from the real workpiece geometry so that there is no influence of position and shape errors on the deburring quality. However, for complex workpiece geometries, teaching is a time-consuming procedure and surface or contour reconstruction needs complex computations.

Other research focuses on a precise object localization to adapt the robot tool-path [1], [12]. In this case, the workpiece is only roughly positioned within the robot workspace and can be registered using sensor data and its nominal CAD-model. The most popular approach for solving the registration problem is the Iterative Closest Point (ICP) algorithm introduced by Besl and McKay [13]. It iteratively minimizes the sum of squared distances between points in a dataset and the closest points in a model to compute the rigid transformation for the alignment of the two datasets. The perfomance of the ICP algorithm for non-deformed datasets is analysed in [14]. Many variants of the ICP approach exist, e.g. Segal et al., who propose a generalization of the ICP algorithm that also takes into account the locally planar surface structure of both datasets to increase robustness in the case of measurement noise and outliers [15]. However, inaccuracies of upstream manufacturing processes, like e.g. milling or drilling, can result in geomet-

Peer-review under responsibility of the scientific committee of the 49th CIRP Conference on Manufacturing Systems

doi:10.1016/j.procir.2016.11.094

ric shape deviations between nominal CAD model and sensor data of the manufactured part resulting in inaccuracies of the registration process. Considering high-precision deburring of contours, these deviations are not negligible and should be included in the registration procedure.

The precise registration of deformed parts based on ICP methods is widely discussed in the field of Computer Aided Inspection (CAI). A method for extending the ICP algorithm to align a point cloud with a CAD model based on the original surface model and instantaneous kinematics is proposed in [16]. An efficient ICP algorithm to register point clouds with a surface mesh model and a data structure to combine nearest nodes and topological neighbour facets is proposed in [17]. A modified ICP algorithm for automated shape inspection based on region-based triangulation for capturing of part deviations is discussed in [18]. However, these approaches only focus on the analysis of shape deviations for quality evaluation but do not create an updated product model representing the actual workpiece shape.

Registering of deformable objects can be achieved by extended shape deformation models with differential-geometric constraints [19], [20], [21], [22], with projection functions [23], [24] or by integration of the physical behaviour with finite element methods (FEM) [25], [26]. The drawback of these methods however lies in the complexity of these models and the problems that arise in industrial applications in terms of fast and robust integration.

In this paper, a novel, easy to implement and practical approach is proposed to detect shape deviations of workpieces for automatic adaptation of robotic deburring processes. The approach only uses dimensional tolerance specifications of the manufactured part provided by the product design and a matching process based on the generalized ICP algorithm by [15]. This contribution is structured as follows: Chapter 2 describes the approach for detection of workpiece shape deviations to adapt the tool path in robotic deburring processes. In Chapter 3 implementation details are presented and possible influences on a correct detection of shape deviations are analyzed. In Chapter 4 the developed approach is validated by a virtual test case and by experiments on a real robotic deburring process. Finally conclusions are presented in Chapter 5.

2. Approach

The proposed approach focuses on the detection of shape deviations between nominal CAD model and 3D sensor data of a manufactured part to adapt the trajectory planning of the tool path along a workpiece edge contour. Fig. 1 shows the setup of a robotic deburring system equipped with deburring tool and 3D sensor and the influence of workpiece shape deviations on the deburring contour and the object localization process.

The concept of our approach is shown in Fig. 2. In a first step, a set of reference CAD models is generated representing variations of the nominal product geometry. To derive these samples from the nominal CAD model additional information about manufacturing tolerances is used. This information is typically provided by the technical drawings of a product. It describes the acceptable deviations between the nominal product design and the workpiece geometry after a manufacturing process to guarantee the correct product function. These tolerances

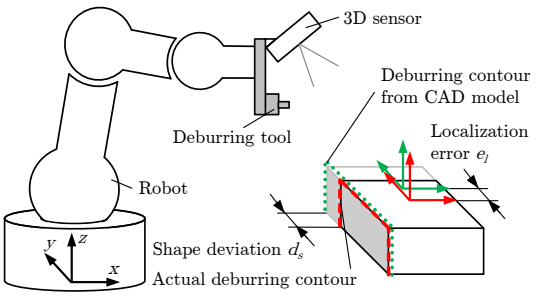

Fig. 1. Influence of workpiece shape deviations on deburring contour and object localization.

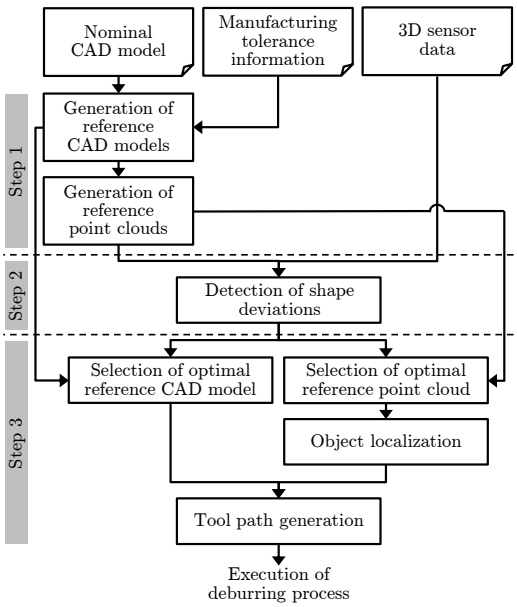

Fig. 2. Concept for detection of shape deviations for tool path adaptation in robotic deburring.

however might be beyond acceptable limits for the correct execution of an automated deburring process using a CAD-based trajectory planning. In the presented approach, we use information about dimensional tolerances to generate possible variations of the workpiece geometry model like shown in Fig. 3. For a given nominal dimension w, the upper and lower tolerance values t_u and t_l can be used to generate different dimension variations w_i and hence different geometry models:

$$w_i = w + t_l + \frac{t_u - t_l}{n-1} \cdot (i-1) \tag{1}$$

with $i = 1, ..., n$ and $n \geq 2$. The generation of reference CAD models can be performed manually or automatically if the tolerance information is added to the CAD model during the design phase. From the reference CAD models, a set of related reference point clouds is derived. Before each specific deburring task, it has to be identified which tolerances have a possible influence on the geometry of the deburring contour. As the calculation time for the deviation detection increases for the number of reference models, the quantity of reference models should be

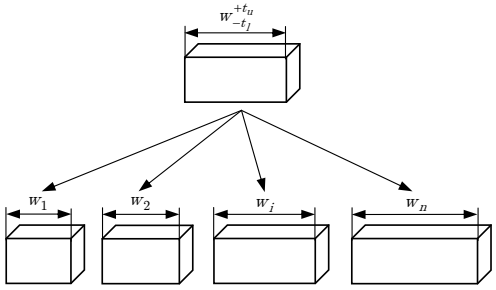

Fig. 3. Generation of reference CAD models representing variations of the nominal workpiece geometry within given tolerance values.

kept as small as possible to find a balance between the required deburring quality and cycle time.

In the second step, a matching process is performed between the point clouds for each of the considered reference variants and the point cloud obtained from measuring the manufactured workpiece using an ICP algorithm. Resulting point distances of corresponding points in the two datasets of each matching process are used for evaluation of shape similarity. The basic idea is that ceteris paribus the average Euclidean distance between corresponding points decreases the more similar the geometry of the reference point cloud is to the actual workpiece geometry. As a result, the optimal reference point cloud and the related reference CAD model can be identified.

In the final step, the tool path is generated based on the identified reference CAD model using typical CAD/CAM software. Moreover, the workpiece is localized by performing a matching process between the identified reference point cloud and 3D sensor data of the workpiece to transform the trajectory to the actual workpiece location.

3. Implementation

Our objective is to detect shape deviations between a reference point cloud derived from the workpiece CAD model and a sensor point cloud obtained from a 3D measurement of the manufactured workpiece. Let $R_i = \{\vec{r}_{i,j}\}$ be the reference point cloud with $i = 1, ..., n$ different dimension variants (see Equ. (1)) and $S = \{\vec{s}_k\}$ be the sensor point cloud with the points $\vec{r}_{i,j}$ and $\vec{s}_k$ for $j = 1, ..., N_R$ and $k = 1, ..., N_S$. In order to align each reference point cloud R_i with the sensor point cloud S, a matching process is performed using the generalized ICP algorithm by [15]. It iteratively minimizes the sum of squared distances between corresponding points in R_i and S taking into account locally planar structure to align R_i with S. However, if there are shape deviations between the underlying geometry models, the alignment cannot be performed accurately. To identify the reference point cloud R_i out of n different variants that has the highest geometric similarity with the sensor point cloud S, the average Euclidean distances after each matching process can be compared. The closest distance between a point $\vec{s}_k$ to a corresponding point in R_i is expressed by:

$$d(\vec{s}_k, R_i) = \min d(\vec{s}_k, \vec{r}_{i,j}) \tag{2}$$

We introduce a similarity function $SF(i)$ that is defined as the average Euclidean distance between each point in S and its nearest neighbour in R_i after the matching process for each dimension variant i of the reference models:

$$SF(i) = \frac{1}{N_S} \sum_{k=1}^{N_S} \min d(\vec{s}_k, \vec{r}_{i,j}) \tag{3}$$

With other things the same, $SF(i)$ has to decrease if the point cloud matching is performed with a reference point cloud R_i that is more similar to S.

In the following, different influences on the similarity function $SF(i)$ are considered. The reference point clouds are derived from the workpiece CAD model and we suppose a quadratic grid of points with grid size q on the object surfaces, like shown in Fig. 4 (a). In real applications, an optical 3D sensor typically delivers irregulary sampled point cloud data of the measured surfaces due to its measuring principle and additional sensor noise. So we assume a random and uniform distribution of the sensor points $\vec{s}_k$ on the workpiece surfaces as also shown in Fig. 4 (a).

Assuming the two point sets lying on the same surface, as it is the case in the absence of shape deviations, the distance between a single point $\vec{s}_k$ and the nearest corresponding point $r_{i,j}$ in R_i is shown in Fig. 4 (b) and can be expressed as

$$d(\vec{s}_k, R_i) = \sqrt{x_k^2 + y_k^2} \tag{4}$$

where $x_k, y_k = -\frac{q}{2}, ..., \frac{q}{2}$. For a random and uniform distribution of the points $\vec{s}_k$ and the number of points in the sensor point cloud $N_S \to \infty$, the minimum value of $SF(i)$ can be expressed as a function of the grid size q by the surface integral

$$\begin{aligned} \min SF(i) &= q \cdot \tfrac{1}{2} \int_0^1 \int_0^1 \sqrt{x^2 + y^2} dx dy \\ &= q \cdot c \end{aligned} \tag{5}$$

with the constant value c ≈ 0.3826. This means that the expected minimum value of $SF(i)$ can be calculated as a func-

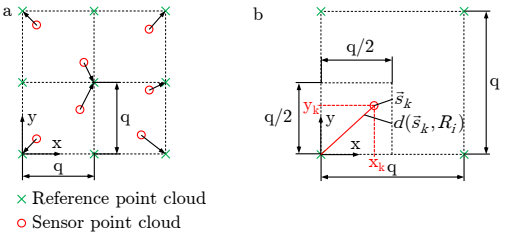

Fig. 4. (a) Distribution of reference and sensor point cloud on a plane surface; (b) Distance of randomly distributed point to quadratic point raster.

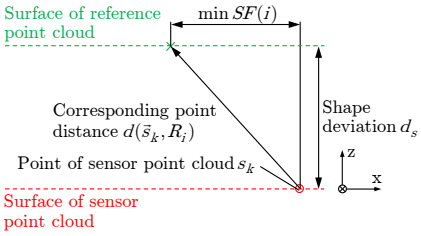

Fig. 5. Dependency of corresponding point distance on shape deviations.

tion of the grid size q of the reference point cloud R_i. However, in the case of shape deviations, a point s_k does not lie on the same surface as the reference point cloud R_i, like shown in Fig. 5. Here, the distance $d(\vec{s}_k, R_i)$ also depends on the distance d_s between the points $\vec{s}_k$ in the sensor point cloud and the corresponding surface of the reference point cloud R_i, which can be expressed as:

$$d(\vec{s}_k, R_i) = \sqrt{(q \cdot c)^2 + d_s^2} \tag{6}$$

The distance d_s can be interpreted as the shape deviation between S and R_i. This means that according to Equ. (3) the value of $SF(i)$ increases with increasing shape deviation. Moreover, the gradient of $SF(i)$ for a given shape deviation increases with decreasing values of the grid size q of the reference point clouds. According to Equ. (3), the similarity function $SF(i)$ is defined as the average of all minimum distances between the sensor points s_k and the reference point cloud R_i. Thus, the gradient of $SF(i)$ also increases with an increasing ratio of the number of points that are affected by the deviation to all points captured by the sensor. This means that in real applications the sensor view field should be defined in a way that as many captured points as possible are affected by the shape deviations to get significant results of $SF(i)$ and enable a robust deviation detection.

4. Experimental Validation

The validation of the proposed approach is performed on a notch contour of a typical deburring workpiece with given tolerance values as shown in Fig. 6.

4.1. Virtual Test Case

In a first test case, virtual sensor data is used, so that an evaluation without additional influences, like e.g. sensor noise, can be performed. The sensor point cloud S is generated from the nominal CAD model without shape deviations. The points of S are randomly distributed on the object surfaces with an average point distance of 0.2 *mm* which corresponds to the resolution of the 3D sensor in our real robot system. Moreover, a set of $n = 11$ reference CAD models is derived from the nominal CAD model of the test workpiece according to Equ. (1) representing different shape variations within the given tolerance values. With the upper tolerance value $t_u = +0.3$ *mm* and the lower tolerance value $t_l = -0.3$ *mm* the difference between dimensions of each of the generated models is 0.06 *mm*. These

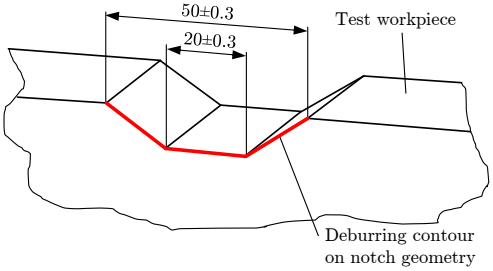

Fig. 6. Geometry of test workpiece including tolerance information.

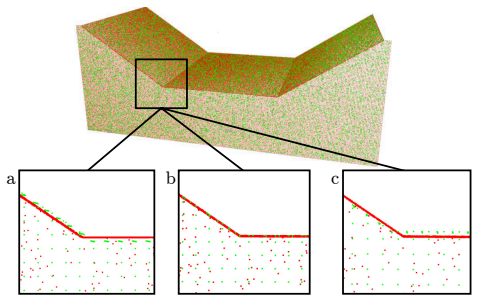

Fig. 7. Result of point cloud matching between sensor points (red) and reference points (green) with (a) minimum tolerance; (b) nominal; and (c) maximum tolerance values.

geometry models are used to generate corresponding reference point clouds R_i with a quadratic grid of points on the object's surfaces, like presented in Chapter 3. We limit the point cloud matching with the generalized ICP algorithm to 50 iterations since convergence is typically reached before. The results of the matching process between the virtual sensor data and the reference point clouds R_1 with minimum, R_6 with nominal and R_{11} with maximum dimensions and a grid size of $q = 0.2$ *mm* are shown in Fig. 7.

To evaluate the influence of the grid size on the similarity function $SF(i)$, several sets of reference clouds R_i are generated, each set with a different grid size q. As the virtual sensor data is generated from the nominal CAD model, the minimum value of $SF(i)$ for each reference cloud set is expected for $i = 6$ corresponding to a reference cloud without shape deviations. The values of $SF(i)$ for the different grid sizes are presented in Fig. 8 and show that the deviation detection in this test case provides correct results until a grid size of $q \leq 0.5$ *mm*. The gradient of $SF(i)$ decreases with increasing grid size q as described in Chapter 3 which leads to numeric calculation errors for higher grid sizes. The results also show that the minimum values of $SF(i)$ correspond to the expected values according to Equ. (5). For $q = 0.5$ *mm* the reference point clouds R_i have around 9.500 points. The computations for the shape deviation detection are performed with an Intel quad-core processor 2.8 GHz and 16 GB RAM, which leads to a calculation time of around 11 seconds for $n = 11$ dimension variants.

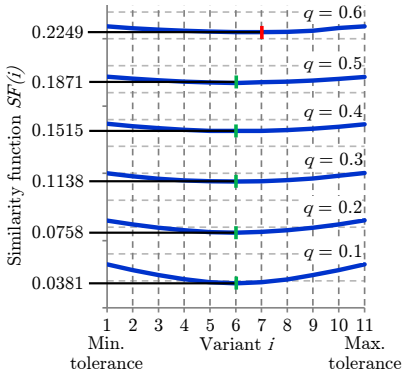

Fig. 8. Results of similarity function $SF(i)$ for virtual sensor data and reference point clouds with different grid size q.

4.2. Test Case with Robotic Deburring System

The proposed method is also validated with a robotic deburring system shown in Fig. 9. The end effector of the 6-axis industrial robot is equipped with a 3D stereo camera to obtain real sensor data of the workpiece geometry and a milling tool to perform the deburring process. The 3D camera provides a point cloud with 360.000 points per measurement and has an optimum x-y view field of 155×118 *mm*, which corresponds to an average point distance of around 0.2 *mm* in the x-y plane. The test workpiece is made of non-alloy structural steel S355JR. It is manufactured with tight tolerances of $t_u = +0.02$ *mm* and $t_l = -0.02$ *mm* compared to its original tolerance information in Fig. 6 to guarantee that the workpiece geometry in the test scenario is close to its nominal CAD model. The testing is performed with the same sets of reference point clouds as in the virtual test case in Chapter 4.1. This allows to assess the influence of the grid size q of the reference clouds on the values of $SF(i)$ under real conditions in the robotic deburring scenario. As the test workpiece geometry is close to its nominal CAD model, the expected result of the shape deviation detection is a minimum value of $SF(i)$ for $i = 6$ corresponding to a reference point cloud without shape deviations. The results of $SF(i)$ for different grid sizes q are shown in Fig. 10.

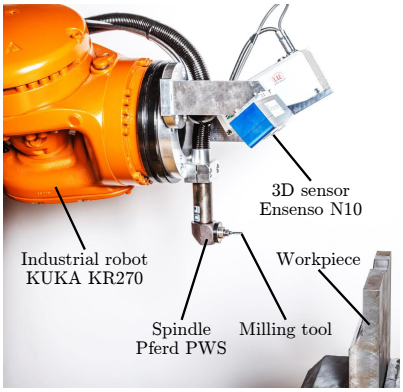

Fig. 9. Experimental setup with deburring tool and 3D sensor.

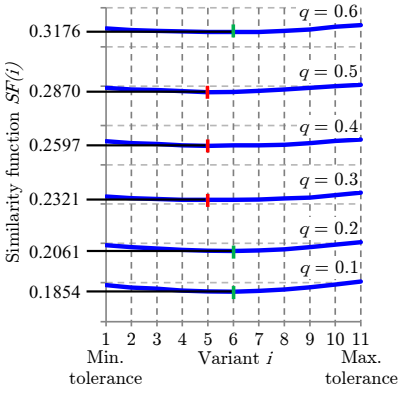

Fig. 10. Results of similarity function $SF(i)$ for real sensor data and reference point clouds with different grid size q.

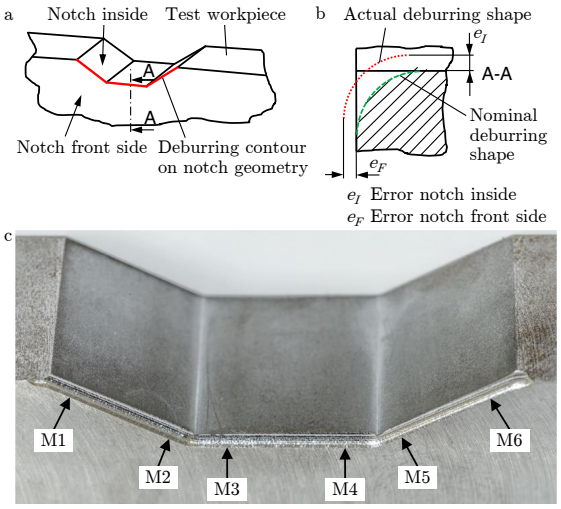

Fig. 11. (a) Notch geometry; (b) Possible errors on deburring contour; (c) Test workpiece after deburring process with detection of shape deviations and measurement positions M1 to M6.

As in the test case with virtual sensor data, the results in this real test case also indicate the increasing significance of the $SF(i)$ with decreasing grid size q of the reference clouds. Due to additional influences, like sensor noise, the $SF(i)$ in this test scenario only provides correct results until a grid size of $q \leq 0.2$ *mm*. This corresponds to a reference point cloud R_i with around 55.000 points and a calculation time of around 30 seconds for $n = 11$ dimension variants. In other deburring scenarios with different sensors and workpiece geometries, this evaluation has to be performed again to obtain the minimum required grid size of the reference point clouds for a correct shape deviation detection. To showcase the effect of the shape deviation detection on the quality of a real deburring process, three experiments are performed. The first test is based on the nominal reference geometry, which in this case has been identified as the appropriate reference model after the detection of shape deviations. The second one is performed using a geometry model with minimum deviations respective to the given tolerance information. The third experiment is based on a geometry model with maximum deviations. The deburring process is performed by generating several facets on the deburring contour in order to reach a rounding of the edge. The deburring contour with the definition of possible errors is shown in Fig. 11 (a) and (b). The deburred edge on the test workpiece is shown in Fig. 11 (c) indicating also six measurement positions for a subsequent quality measurement of the deburring shape.

The results of the quality measurement are presented in Table 1 for the different test cases and the corresponding measurement positions. The standard deviation error for the first test case with deviation detection is around 32% smaller than the second test case and around 57% smaller than the third test case. The remaining inaccuracies can be interpreted as the result of a combination of additional error sources, like e.g. the calibration of the sensor, the calibration of the deburring tool and the path accuracy of the robot. However, the results indicate an increased deburring quality using the proposed approach for detection of shape deviations.

Table 1. Results of quality measurements on deburred edges.

Measurement Position M	Error e_l (Test with deviation detection)	Error e_l (Test without deviation detection and min. tolerance)	Error e_l (Test without deviation detection and max. tolerance)
1	0.076	-0.048	0.068
2	0.000	-0.140	0.000
3	0.064	0.000	-0.048
4	0.000	-0.036	-0.100
5	0.028	-0.044	0.100
6	0.040	-0.076	0.040
Standard Deviation	0.032	0.047	0.075

5. Conclusion and Future Work

We have proposed a novel approach for detection of workpiece shape deviations to adapt the tool path in a robotic deburring system. Dimensional tolerance information of manufactured parts provided by the product design was used to generate variants of the workpiece CAD model and corresponding reference point clouds. A matching process based on an ICP algorithm was performed between each of the reference clouds and a measured point cloud from the manufactured part. The shape similarity between compared point clouds was assessed by evaluation of corresponding point distances. Finally, the most similar geometry model was selected for subsequent trajectory planning and workpiece localization. As the approach depends on the actual system setup, like used sensors and workpieces, this paper shows how to implement the shape deviation detection for a new deburring scenario. Experimental validation of the proposed approach was performed by a virtual test case and by using an industrial robot equipped with a stereo camera for shape sensing and a milling tool for subsequent execution of the deburring process. The results of deburring a test workpiece of non-alloy structural steel show an increased deburring quality and a reduction of the standard deviation error on the deburring contour of around 32%. Deviations of deburring contour dimensions have been identified with an accuracy of 0.06 mm.

Future work will focus on detection of shape deviations on more complex workpiece geometries with different tolerance types. Moreover, concepts for fast and efficient computation of the shape deviation detection will be developed.

Acknowledgements

The research leading to these results has received funding from the European Union Seventh Framework Program (FP7/2007-2013) under grant agreement no. 287787.

References

[1] Song, H.C., Kim, B.S., Song, J.B.. Tool path generation based on matching between teaching points and CAD model for robotic deburring. In: IEEE/ASME Int Conf on Adv Intelligent Mechatronics. 2012, p. 890–895.
[2] Wang, X., Wang, Y., Xue, Y.. Adaptive control of robotic deburring process based on impedance control. In: IEEE Int Conf on Industrial Informatics. 2006, p. 921–925.
[3] Robertsson, A., Olsson, T., Johansson, R., Blomdell, A., Nilsson, K., Haage, M., et al. Implementation of industrial robot force control case study: high power stub grinding and deburring. In: IEEE/RSJ Int Conf on Intelligent Robots and Systems. 2006, p. 2743–2748.
[4] Pagilla, P.R., Yu, B.. Adaptive control of robotic surface finishing processes. In: IEEE American Control Conference; vol. 1. 2001, p. 630–635.
[5] Li, C., Park, C., Kyung, J., Chung, G., Han, C.. Study on teaching path reconstruction algorithm based direct teaching and playback method. In: IEEE 8th Int Conf on Ubiquitous Robots and Ambient Intelligence (URAI). 2011, p. 778–779.
[6] Lee, S., Li, C., Kim, D., Kyung, J., Han, C.. The direct teaching and playback method for robotic deburring system using the adaptive force-control. In: IEEE Int S on Assembly and Manufacturing. 2009, p. 235–241.
[7] Schraft, R., Meyer, C.. The need for an intuitive teaching method for small and medium enterprises. VDI Berichte 2006;1956:95.
[8] Solvang, B., Sziebig, G., Korondi, P.. Vision based robot programming. In: IEEE Int Conf on Networking, Sensing and Control. 2008, p. 949–954.
[9] Bi, Z., Kang, B.. Sensing and responding to the changes of geometric surfaces in flexible manufacturing and assembly. Enterprise Information Systems 2014;8(2):225–245.
[10] Park, S.C., Chung, Y.C.. Tool-path generation from measured data. Computer-Aided Design 2003;35(5):467–475.
[11] Zhang, H., Chen, H., Xi, N., Zhang, G., He, J.. On-line path generation for robotic deburring of cast aluminum wheels. In: IEEE/RSJ Int Conf on Intelligent Robots and Systems. 2006, p. 2400–2405.
[12] Dietz, T., Schneider, U., Barho, M., Oberer-Treitz, S., Drust, M., Hollmann, R., et al. Programming system for efficient use of industrial robots for deburring in SME environments. In: VDE 7th German Conf on Robotics; Proceedings of ROBOTIK 2012. 2012, p. 1–6.
[13] Besl, P., McKay, N.D.. A method for registration of 3-d shapes. IEEE Trans Pattern Analysis and Machine Intelligence 1992;14(2):239–256.
[14] Ezra, E., Sharir, M., Efrat, A.. On the performance of the ICP algorithm. Computational Geometry 2008;41(1):77–93.
[15] Segal, A., Haehnel, D., Thrun, S.. Generalized-ICP. In: Robotics: Science and Systems; vol. 2. 2009,.
[16] Pottmann, H., Wallner, J., Leopoldseder, S.. Kinematical methods for the classification, reconstruction, and inspection of surfaces. Congrès national de mathématiques appliquées et industrielles 2001;:51–60.
[17] Zhu, L., Barhak, J., Srivatsan, V., Katz, R.. Efficient registration for precision inspection of free-form surfaces. Int J Advanced Manufacturing Technology 2007;32(5-6):505–515.
[18] Ravishankar, S., Dutt, H., Gurumoorthy, B.. Automated inspection of aircraft parts using a modified ICP algorithm. Int J Advanced Manufacturing Technology 2010;46(1-4):227–236.
[19] Li, M., Kambhamettu, C., Stone, M.. Nonrigid motion recovery for 3d surfaces. Image and Vision Computing 2007;25(3):250–261.
[20] Kambhamettu, C., Goldgof, D., He, M., Laskov, P.. 3d nonrigid motion analysis under small deformations. Image and Vision Computing 2003;21(3):229–245.
[21] Laskov, P., Kambhamettu, C.. Curvature-based algorithms for nonrigid motion and correspondence estimation. IEEE Trans Pattern Analysis and Machine Intelligence 2003;25(10):1349–1354.
[22] Papazov, C., Burschka, D.. Deformable 3d shape registration based on local similarity transforms. In: Computer Graphics Forum; vol. 30. Wiley Online Library; 2011, p. 1493–1502.
[23] Béarée, R., Dieulot, J.Y., Rabaté, P.. An innovative subdivision-ICP registration method for tool-path correction applied to deformed aircraft parts machining. Int J Adv Manuf Technology 2011;53(5-8):463–471.
[24] Amberg, B., Romdhani, S., Vetter, T.. Optimal step nonrigid ICP algorithms for surface registration. In: IEEE Conf on Computer Vision and Pattern Recognition. 2007, p. 1–8.
[25] Zhong, H., Kim, J., Li, H., Nurushev, T., Movsas, B., Chetty, I.J.. A finite element method to correct deformable image registration errors in low-contrast regions. Physics in medicine and biology 2012;57(11):3499.
[26] Krol, A., Unlu, M.Z., Magri, A., Lipson, E., Coman, I.L., Mandel, J., et al. Iterative finite element deformable model for nonrigid coregistration of multimodal breast images. In: IEEE 3rd Int Symposium on Biomedical Imaging: Nano to Macro. 2006, p. 852–855.